Protein Science (2000), *9*:1669–1684. Cambridge University Press. Printed in the USA.

Analysis of the internal motion of free and ligand-bound human lysozyme by use of ^{15}N NMR relaxation measurement: A comparison with those of hen lysozyme

SHOUHEI MINE, TADASHI UEDA, YOSHIO HASHIMOTO, AND TAIJI IMOTO

Graduate School of Pharmaceutical Sciences, Kyushu University, Fukuoka 812-8582, Japan

(RECEIVED February 8, 2000; FINAL REVISION June 7, 2000; ACCEPTED June 16, 2000)

Abstract

Human lysozyme has a structure similar to that of hen lysozyme and differs in amino acid sequence by 51 out of 129 residues with one insertion at the position between 47 and 48 in hen lysozyme. The backbone dynamics of free or $(NAG)_3$-bound human lysozyme has been determined by measurements of ^{15}N nuclear relaxation. The relaxation data were analyzed using the Lipari–Szabo formalism and were compared with those of hen lysozyme, which was already reported (Mine S et al., 1999, *J Mol Biol 286*:1547–1565). In this paper, it was found that the backbone dynamics of free human and hen lysozymes showed very similar behavior except for some residues, indicating that the difference in amino acid sequence did not affect the behavior of entire backbone dynamics, but the folded pattern was the major determinant of the internal motion of lysozymes. On the other hand, it was also found that the number of residues in $(NAG)_3$-bound human and hen lysozymes showed an increase or decrease in the order parameters at or near active sites on the binding of $(NAG)_3$, indicating the increase in picosecond to nanosecond. These results suggested that the immobilization of residues upon binding $(NAG)_3$ resulted in an entropy penalty and that this penalty was compensated by mobilizing other residues. However, compared with the internal motions between both ligand-bound human and hen lysozymes, differences in dynamic behavior between them were found at substrate binding sites, reflecting a subtle difference in the substrate-binding mode or efficiency of activity between them.

Keywords: lysozyme; model-free; NMR relaxation; order parameter

Protein recognition is a critical component of the function of a majority of biological processes. To explain the efficiency of an enzyme, the "induced fit" model of binding was considered, which provides an intuitive picture that reinforces the idea of "freezing out" multiple possible conformations upon binding. Molecular dynamic simulations and NMR relaxation data of barstar (Wong & Daggett, 1998) supported the conventional idea that certain residues in apo forms were more flexible than in the ligand-bound states. However, the increase in motion of a protein upon binding has been reported by using NMR relaxation in a few proteins, 4-oxalocrotonate tautomerase (Stivers et al., 1996), hen lysozyme (Mine et al., 1999a), and mouse major urinary binding protein I (Zidek et al., 1999). Under the circumstances, whether the motion of protein upon binding increases or decreases is controversial.

Among the methods available for characterizing the protein conformational dynamics in solution, only NMR relaxation measurement can provide detailed experimental information on the mobility of each amino acid residue in the protein. Relaxation data are analyzed using the Lipari–Szabo formalism (Lipari & Szabo, 1982a, 1982b), which allows the extraction of the overall correlation time (τ_c), internal correlation time (τ_e), and generalized order parameters (S^2) for backbone N–H bond vectors. Proteins have various types of internal motion that are hierarchically composed on a different timescale from picosecond to hour. It has been considered that such internal motions of proteins may be very important for their biological function as has been shown in enzyme catalysis and protein–ligand interactions. Therefore, it is necessary to investigate the relationship between the biological function and the internal motion of a protein. Proteins with substantial similarity in their primary structures are almost certain to have arisen from a common ancestor during evolution, and they have invariably been found to have very similar folded conformations (Creighton, 1984). Therefore, one of the approaches to investigate the relationship

Reprint requests to: Taiji Imoto, Graduate School of Pharmaceutical Sciences, Kyushu University, 3-1-1 Maidashi, Higashi-ku, Fukuoka 812-8582, Japan; e-mail: imoto@imm.phar.kyushu-u.ac.jp.

Abbreviations: HSQC, heteronuclear single quantum coherence; NOE, nuclear Overhauser effect; NOESY, NOE spectroscopy; T_1, longitudinal relaxation time; T_2, transverse relaxation time; $D_\parallel/D_\perp$, rotational diffusional anisotropy defined as $2D_z/(D_x + D_y)$ where D is the rotational diffusion coefficient; $(NAG)_3$, tri-*N*-acetyl-chitotrioside; $(NAG)_6$, hexa-*N*-acetyl-chitohexaoside.

```
                5         10        15        20
HUMAN LZ   K V F E R C E L A R T L K R L G M D G Y
HEN LZ     - - - G - - - - - A A M - - H - L - N -

                25        30        35        40
HUMAN LZ   R G I S L A N W M C L A K W E S G Y N T
HEN LZ     - - Y - - G - - V - A - - F - - N F - -

                45        50        55        60
HUMAN LZ   R A T N Y N A G D R S T D Y G I F Q I N
HEN LZ     Q - - - R - T * - G - - - - - - L - - -

                65        70        75        80
HUMAN LZ   S R Y W C N D G K T P G A V N A C H L S
HEN LZ     - - W - - - - - R - - - S R - L - N I P

                85        90        95        100
HUMAN LZ   C S A L L Q D N I A D A V A C A K R V Y
HEN LZ     - - - - - S S D - T A S - N - - - K I V

                105       110       115       120
HUMAN LZ   R D P Q G I R A W V A W R N R C Q N R D
HEN LZ     S - G N - M N - - - - - - - - - K G T -

                125       130
HUMAN LZ   V R Q Y V Q G C G V
HEN LZ     - Q A W I R - - R L
```

Fig. 1. Alignment of human and hen lysozyme sequences. For hen lysozyme, nonidentical residues are indicated relative to those of human lysozyme. The asterisk (*) indicates the deleted position in hen lysozyme.

between biological function and the internal motion of a protein is to compare the internal motions of enzymes whose tertiary structures are similar but their efficiencies of activity are different. Human lysozyme is an enzyme consisting of 130 amino acid residues with four disulfide bonds. Human and hen lysozyme have a relatively high sequence homology differing by 51 out of 129 amino acid residues and the insertion of a Gly at position 48 (Fig. 1). In addition, X-ray structures of both lysozymes were available at high resolution and were very similar (Artymuik & Blake, 1981; Handoll, 1985). However, human lysozyme had a higher activity against a glycol chitin, a lysozyme substrate, than hen lysozyme (Kuramitsu et al., 1974). To date, the internal motions of human lysozyme have not been reported in solution, whereas those in hen lysozyme in various solution conditions have been investigated (Buck et al., 1995a, 1995b; Schwalbe et al., 1997). Thus, we analyzed the backbone dynamics of free and substrate analogues, $(NAG)_3$-bound human lysozyme with a ^{15}N relaxation measurement and then compared with those of hen lysozyme to understand the relationship between the internal motions and structural similarities.

Results

^1H–^{15}N chemical shift assignment

Backbone assignments of free and $(NAG)_3$-bound human lysozyme were carried out by comparing cross-peak resonances from three-dimensional (3D) NOESY-HSQC NMR spectra by reference to the published assignments for human lysozyme (Ohkubo et al., 1991). As a result, we completed the backbone ^{15}N signal assignment, but slight shift deviations were found in some residues by comparing with previous assignments due to differences in temperature and pH.

The chemical shifts of resonances of ligand-bound human lysozyme showed small changes, and many of their resonances were broadened as a result of a chemical exchange effect. The residues that were not detected due to signal broadening were N27, L31, A32, Q58, N60, Y63, W64, C65, D67, D87, V99, V100, D102, R107, W109, V110, Q117, and V130. The X-ray crystallographic studies of human lysozyme and its complex with oligosaccharides indicated that the active site involves a cleft that built up six substrate binding subsites denoted as subsites A to F, and $(NAG)_3$ occupied subsites A, B, and C or B, C, and D (Matsushima et al., 1990). We confirmed that the NH protons whose signals slightly shifted and decreased in intensity were located around the active site cleft, particularly subsites A, B, C, and D. This result is consistent with the results that have been reported previously (Ohkubo et al., 1991) and indicated that $(NAG)_3$ was in slow exchange on the chemical shift timescale at this condition.

The internal motion of free human lysozyme elucidated by ^{15}N spin relaxation

The relaxation parameters were measured for 125 out of 130 amide groups of human lysozyme in the free state (Fig. 2). The resonances of K1, P71, and P103 could not be detected and reliable values of relaxation parameters for some residues (W28, V74) could not be calculated due to severe spectral overlap.

The first task in extracting motional information from relaxation parameters is to determine the parameters that define the overall rotational motion of the molecule. The ratio of diffusion tensor is $D_\parallel/D_\perp = 1.3$ for hen lysozyme, and this indicated that the rotational diffusion is close to isotropic. Indeed, model free analysis of hen lysozyme was carried out under this assumption (Buck et al., 1995a; Mine et al., 1999a), and this may also be applicable to human lysozyme because human lysozyme has a folded structure similar to that of hen lysozyme. However, we must pay attention to use the "model-free" approach because the presence of rotational diffusion anisotropy could be misidentified as conformational exchange (Tjandra et al., 1995, 1996). It is reported that hen lysozyme has moderate anisotropy (Boyd & Redfield, 1998), and this means that slight anisotropic diffusion could be reflected in the relaxation data. But it is well known that anisotropic tumbling would hardly influence the values of the overall rotational correlation time, the order parameters, or the internal correlation times (Tjandra et al., 1995; Gagne et al., 1998; Prompers et al., 1999; Zidek et al., 1999) because of the insensitivities of the order parameter to the orientation of the NH bond relative to the long axis of the diffusion tensor for $D_\parallel/D_\perp \approx 1.3$ (Zhang et al., 1998). From the results of the calculation of the T_1/T_2 ratio (data not shown), significantly large values in T_1/T_2 ratio were not observed for residues residing in a secondary structure. Thus, we assumed that the rotation of the molecule was isotropic. However, to avoid misunderstanding the conformational exchanges, we decided to discuss only the values of the order parameter.

According to the Lipari–Szabo model-free formalism of the spectral density function (Lipari & Szabo, 1982a, 1982b), we obtained the motional parameters from these relaxation data. In this analysis, we applied the five types of model-free spectral density functions that are shown in Table 1 and optimized them by fitting the functions to the experimental data. The overall rotational correlation time τ_c of human lysozyme was evaluated to be 4.97 ns

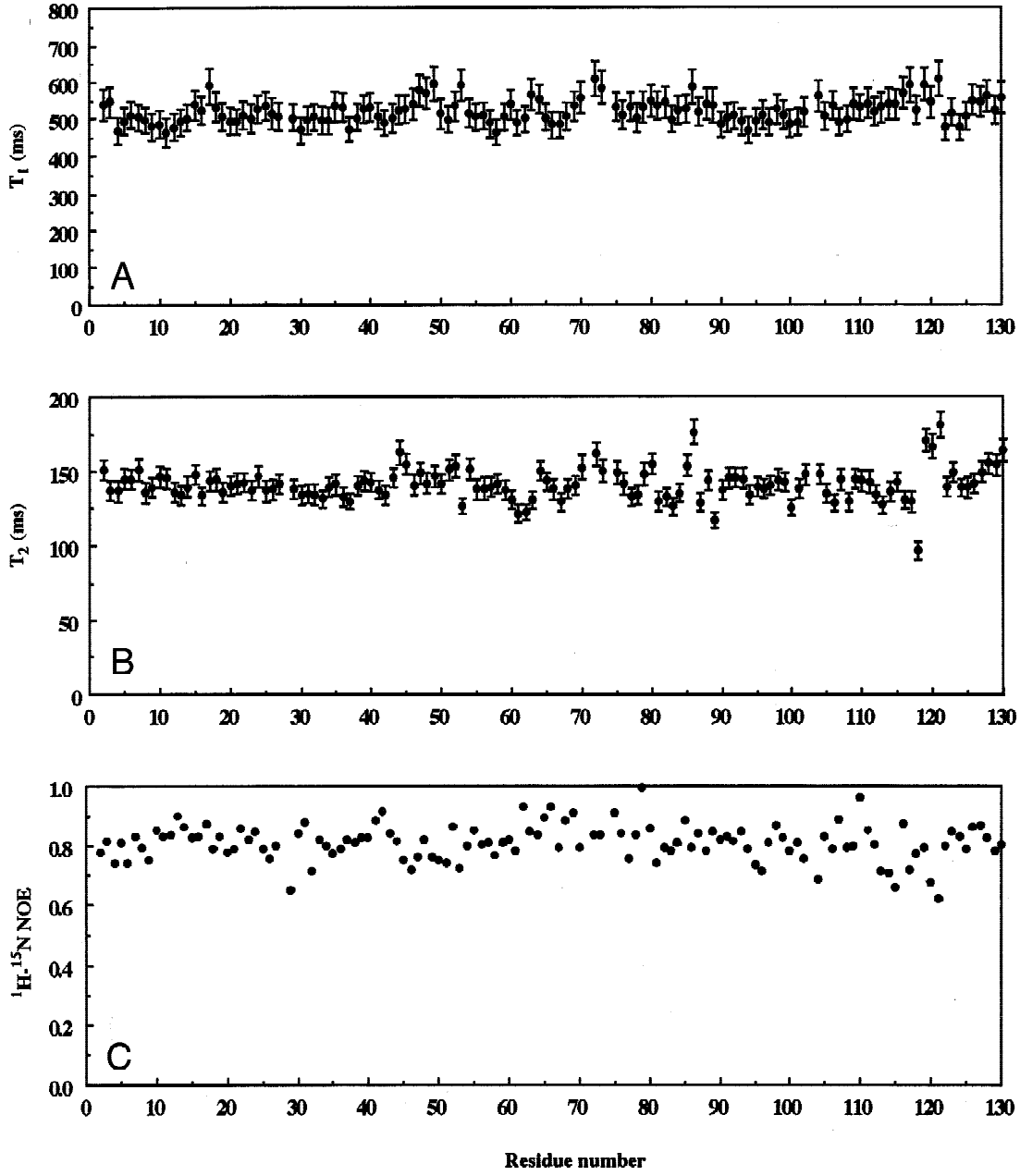

Fig. 2. (**A**) T_1, (**B**) T_2, and (**C**) heteronuclear NOE of the human lysozyme at pH 3.8 and 35 °C.

from the T_1/T_2 values. The obtained motional parameters and the spectral density models used to fit the data are summarized in Figure 3 and Table 2A. For most residues in human lysozymes, the order parameters (S^2) were in the range 0.8–1.0, indicating that the internal motion of human lysozyme was essentially well ordered except for some residues. In contrast, lower order parameters (below 0.8) were observed for M17 (the loop A–B), N44, Y45 (strand 1), D49 (turn 1), S51, D53 (strand 2), Q58 (turn 2), Y63, G72, A73 (long loop), S80, Q86 (near the termini of 3_{10} (i)), C116 (C-terminus of helix D), Q117, R119 (loop D-3_{10} (ii)), D120, V121 (3_{10} (ii)), C128, and V130 (C-terminus). The most flexible region among those described above was around 3_{10} (ii) where the order parameter was below 0.7.

Table 1. *Summary of the spectral density function models used for the optimization of the model-free motional parameters*

Model	Data used in fitting	Optimized parameters[a]
1	T_1, T_2	S^2
2	T_1, T_2	S^2, R_{ex}
3	T_1, T_2, NOE	S^2, τ_e
4	T_1, T_2, NOE	S_f^2, S_s^2, τ_s
5	T_1, T_2, NOE	S^2, τ_e, R_{ex}

[a]The optimization was done with our in-house program RxAnly on a Sun Sparc20 workstation.

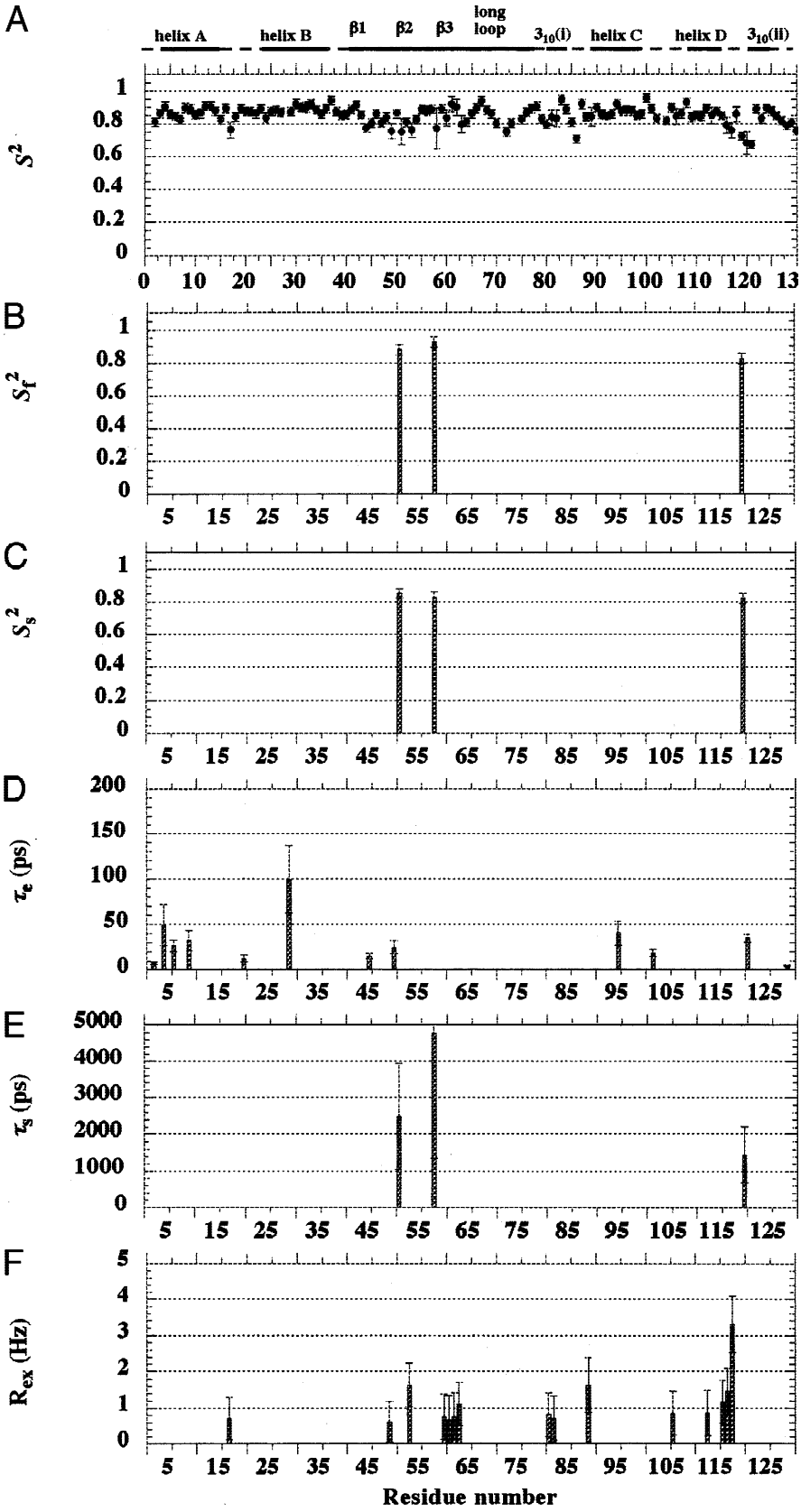

Fig. 3. Extracted model-free parameters of free human lysozyme by parameter optimization with the program RxAnly. **A:** Generalized order parameters S^2. **B:** Order parameters of the fast internal motion S_f^2. **C:** Order parameters of the slow internal motion S_s^2. **D:** Effective correlation times τ_e. **E:** Slow internal correlation times τ_s. **F:** Chemical exchange contributions represented in the broadened linewidth R_{ex}.

Table 2. *Derived order parameter and goodness of fit values for the (A) free and (B) ligand-bound human lysozyme*

Residue	Model	S^2	τ_e	R_{ex}	S_f^2	S_s^2
			A. Free human lysozyme			
K1						
V2	3	0.809 ± 0.025	7.045 ± 1.458			
F3	1	0.863 ± 0.026				
E4	3	0.902 ± 0.028	49.545 ± 22.542			
R5	1	0.855 ± 0.025				
C6	3	0.844 ± 0.025	26.395 ± 6.562			
E7	1	0.825 ± 0.025				
L8	1	0.896 ± 0.027				
A9	3	0.885 ± 0.026	32.230 ± 11.278			
R10	1	0.851 ± 0.025				
T11	1	0.860 ± 0.028				
L12	1	0.905 ± 0.027				
K13	1	0.906 ± 0.027				
R14	1	0.877 ± 0.027				
L15	1	0.823 ± 0.025				
G16	1	0.894 ± 0.026				
M17	2	0.762 ± 0.050		0.708 ± 0.595		
D18	1	0.840 ± 0.027				
G19	1	0.890 ± 0.027				
Y20	3	0.875 ± 0.025	12.546 ± 3.818			
R21	1	0.871 ± 0.026				
G22	1	0.860 ± 0.025				
I23	1	0.889 ± 0.026				
S24	1	0.834 ± 0.026				
L25	1	0.870 ± 0.027				
A26	1	0.878 ± 0.028				
N27	1	0.866 ± 0.025				
W28						
M29	3	0.869 ± 0.026	99.671 ± 37.720			
C30	1	0.918 ± 0.028				
L31	1	0.899 ± 0.027				
A32	1	0.899 ± 0.028				
K33	1	0.917 ± 0.027				
W34	1	0.882 ± 0.026				
E35	1	0.855 ± 0.027				
S36	1	0.892 ± 0.026				
G37	1	0.940 ± 0.026				
Y38	1	0.870 ± 0.026				
N39	1	0.847 ± 0.026				
T40	1	0.850 ± 0.025				
R41	1	0.884 ± 0.025				
A42	1	0.909 ± 0.026				
T43	1	0.848 ± 0.025				
N44	1	0.774 ± 0.026				
Y45	3	0.799 ± 0.024	15.533 ± 2.963			
N46	1	0.854 ± 0.026				
A47	1	0.804 ± 0.025				
G48	1	0.834 ± 0.026				
D49	2	0.754 ± 0.046		0.614 ± 0.568		
R50	3	0.860 ± 0.025	24.693 ± 6.951			
S51	4	0.748 ± 0.077	2,485.809 ± 1,447.305		0.878 ± 0.029	0.852 ± 0.029
T52	1	0.805 ± 0.025				
D53	2	0.760 ± 0.046		1.636 ± 0.584		
Y54	1	0.821 ± 0.026				
G55	1	0.883 ± 0.026				
I56	1	0.878 ± 0.028				
F57	1	0.884 ± 0.025				
Q58	4	0.768 ± 0.123	4,774.817 ± 3,413.644		0.926 ± 0.031	0.829 ± 0.031
I59	1	0.887 ± 0.027				
N60	2	0.833 ± 0.048		0.762 ± 0.626		

(*continued*)

Table 2 (*continued*)

Residue	Model	S^2	τ_e	R_{ex}	S_f^2	S_s^2
			A. Free human lysozyme (continued)			
S61	2	0.915 ± 0.047		0.694 ± 0.662		
R62	2	0.898 ± 0.049		0.777 ± 0.658		
Y63	2	0.793 ± 0.049		1.119 ± 0.609		
W64	1	0.810 ± 0.024				
C65	1	0.859 ± 0.025				
N66	1	0.894 ± 0.027				
D67	1	0.934 ± 0.026				
G68	1	0.880 ± 0.026				
K69	1	0.858 ± 0.026				
T70	1	0.800 ± 0.027				
P71						
G72	1	0.749 ± 0.025				
A73	1	0.799 ± 0.026				
V74						
N75	1	0.823 ± 0.026				
A76	1	0.865 ± 0.027				
C77	1	0.892 ± 0.026				
H78	1	0.901 ± 0.027				
L79	1	0.828 ± 0.026				
S80	1	0.794 ± 0.025				
C81	2	0.836 ± 0.046		0.827 ± 0.612		
S82	2	0.828 ± 0.050		0.713 ± 0.627		
A83	1	0.944 ± 0.026				
L84	1	0.885 ± 0.026				
L85	1	0.806 ± 0.025				
Q86	1	0.707 ± 0.023				
D87	1	0.917 ± 0.027				
N88	1	0.842 ± 0.025				
I89	2	0.840 ± 0.057		1.630 ± 0.742		
A90	1	0.896 ± 0.026				
D91	1	0.850 ± 0.026				
A92	1	0.845 ± 0.026				
V93	1	0.857 ± 0.026				
A94	1	0.917 ± 0.028				
C95	3	0.876 ± 0.025	40.440 ± 12.750			
A96	1	0.878 ± 0.027				
K97	1	0.878 ± 0.026				
R98	1	0.847 ± 0.026				
V99	1	0.858 ± 0.026				
V100	1	0.955 ± 0.026				
R101	1	0.889 ± 0.027				
D102	3	0.830 ± 0.025	18.540 ± 4.333			
P103						
Q104	1	0.816 ± 0.025				
G105	1	0.895 ± 0.026				
I106	2	0.840 ± 0.047		0.856 ± 0.612		
R107	1	0.861 ± 0.026				
A108	1	0.927 ± 0.028				
W109	1	0.837 ± 0.025				
V110	1	0.847 ± 0.026				
A111	1	0.845 ± 0.027				
W112	1	0.892 ± 0.025				
R113	2	0.848 ± 0.048		0.868 ± 0.632		
N114	1	0.875 ± 0.025				
R115	1	0.846 ± 0.025				
C116	2	0.789 ± 0.047		1.171 ± 0.594		
Q117	2	0.759 ± 0.048		1.469 ± 0.626		
N118	2	0.856 ± 0.047		3.312 ± 0.789		
R119	1	0.724 ± 0.023				
D120	4	0.681 ± 0.069	1,446.411 ± 757.491		0.827 ± 0.032	0.823 ± 0.032

(*continued*)

Table 2 (*continued*)

Residue	Model	S^2	τ_e	R_{ex}	S_f^2	S_s^2
			A. Free human lysozyme (continued)			
V121	3	0.674 ± 0.023	34.840 ± 4.388			
R122	1	0.887 ± 0.026				
Q123	1	0.829 ± 0.025				
Y124	1	0.891 ± 0.025				
V125	1	0.877 ± 0.027				
Q126	1	0.845 ± 0.026				
G127	1	0.816 ± 0.025				
C128	1	0.787 ± 0.024				
G129	3	0.803 ± 0.024	4.568 ± 0.897			
V130	1	0.756 ± 0.024				
			B. Ligand-bound human lysozyme			
K1						
V2	1	0.808 ± 0.025				
F3	1	0.932 ± 0.026				
E4	3	0.836 ± 0.028	60.328 ± 17.494			
R5	3	0.802 ± 0.024	52.283 ± 11.065			
C6	3	0.860 ± 0.026	44.003 ± 13.616			
E7	1	0.808 ± 0.025				
L8	1	0.907 ± 0.027				
A9	4	0.799 ± 0.074	2,289.753 ± 1,210.920		0.933 ± 0.031	0.856 ± 0.031
R10	1	0.875 ± 0.026				
T11	1	0.832 ± 0.026				
L12	1	0.900 ± 0.026				
K13	1	0.909 ± 0.026				
R14	3	0.912 ± 0.027	17.650 ± 11.331			
L15	1	0.839 ± 0.026				
G16	1	0.927 ± 0.026				
M17	1	0.810 ± 0.025				
D18	1	0.845 ± 0.026				
G19	1	0.871 ± 0.027				
Y20	1	0.853 ± 0.025				
R21	4	0.780 ± 0.077	1,567.272 ± 497.347		1.019 ± 0.035	0.765 ± 0.035
G22	1	0.888 ± 0.026				
I23	1	0.865 ± 0.025				
S24	3	0.820 ± 0.025	10.529 ± 8.737			
L25	1	0.938 ± 0.029				
A26	1	0.879 ± 0.026				
N27						
W28						
M29	3	0.899 ± 0.024	34.853 ± 13.763			
C30	1	0.886 ± 0.026				
L31						
A32						
K33	1	0.908 ± 0.025				
W34	2	0.826 ± 0.047		1.762 ± 0.772		
E35	1	0.813 ± 0.026				
S36	1	0.852 ± 0.025				
G37	1	0.890 ± 0.024				
Y38	1	0.902 ± 0.025				
N39	1	0.844 ± 0.025				
T40	1	0.911 ± 0.025				
R41	1	0.907 ± 0.026				
A42	1	0.870 ± 0.026				
T43	2	0.798 ± 0.046		1.418 ± 0.726		
N44	3	0.841 ± 0.027	33.309 ± 9.364			
Y45	2	0.788 ± 0.047		1.735 ± 0.675		
N46	2	0.837 ± 0.047		1.125 ± 0.677		
A47	2	0.642 ± 0.045		1.263 ± 0.565		
G48	2	0.684 ± 0.042		1.925 ± 0.595		

(*continued*)

Table 2 (*continued*)

Residue	Model	S^2	τ_e	R_{ex}	S_f^2	S_s^2
			B. Ligand-bound human lysozyme (continued)			
D49	2	0.696 ± 0.045		1.441 ± 0.599		
R50	1	0.839 ± 0.026				
S51	3	0.836 ± 0.025	26.224 ± 7.091			
T52	1	0.811 ± 0.025				
D53	1	1.009 ± 0.030				
Y54	4	0.776 ± 0.073	2,321.126 ± 1,241.884		0.913 ± 0.031	0.851 ± 0.031
G55	2	0.923 ± 0.055		2.378 ± 0.878		
I56	2	0.885 ± 0.044		1.796 ± 0.768		
F57	1	0.999 ± 0.028				
Q58						
I59	1	0.982 ± 0.029				
N60						
S61	2	1.016 ± 0.055		2.258 ± 1.153		
R62	2	0.923 ± 0.051		1.902 ± 0.884		
Y63						
W64						
C65						
N66	1	0.926 ± 0.026				
D67						
G68	1	0.817 ± 0.026				
K69	1	0.874 ± 0.026				
T70	4	0.735 ± 0.079	3,067.079 ± 1,676.007		0.870 ± 0.030	0.845 ± 0.030
P71						
G72	1	0.761 ± 0.023				
A73	3	0.834 ± 0.027	21.761 ± 6.100			
V74						
N75	4	0.669 ± 0.061	1,688.145 ± 680.913		0.822 ± 0.030	0.814 ± 0.030
A76	2	1.068 ± 0.058		2.765 ± 0.990		
C77	2	0.746 ± 0.044		1.691 ± 0.621		
H78	3	0.874 ± 0.026	18.361 ± 7.084			
L79	1	0.849 ± 0.025				
S80	1	0.807 ± 0.026				
C81	4	0.843 ± 0.096	2,671.913 ± 1,131.085		1.059 ± 0.036	0.796 ± 0.036
S82	1	0.906 ± 0.026				
A83	2	0.822 ± 0.045		1.001 ± 0.630		
L84	2	0.826 ± 0.046		0.999 ± 0.638		
L85	1	0.840 ± 0.025				
Q86	4	0.638 ± 0.058	2,231.933 ± 1,090.626		0.752 ± 0.027	0.848 ± 0.027
D87						
N88	1	0.898 ± 0.025				
I89	2	0.820 ± 0.048		0.892 ± 0.660		
A90	1	0.878 ± 0.026				
D91	1	0.868 ± 0.026				
A92	1	0.798 ± 0.027				
V93	2	0.718 ± 0.043		1.455 ± 0.608		
A94	1	0.888 ± 0.028				
C95	3	0.909 ± 0.025	85.377 ± 42.233			
A96	3	0.903 ± 0.026	26.140 ± 11.511			
K97	3	0.894 ± 0.025	81.010 ± 33.618			
R98	1	0.833 ± 0.026				
V99						
V100						
R101	1	0.882 ± 0.025				
D102						
P103						
Q104	2	0.736 ± 0.046		2.308 ± 0.716		
G105	1	1.151 ± 0.035				
I106	2	0.792 ± 0.045		1.008 ± 0.629		
R107						
A108	2	0.883 ± 0.048		1.255 ± 0.753		

(*continued*)

Table 2 (*continued*)

Residue	Model	S^2	τ_e	R_{ex}	S_f^2	S_s^2
B. Ligand-bound human lysozyme (continued)						
W109						
V110						
A111	3	0.851 ± 0.027	39.964 ± 11.988			
W112						
R113	1	0.917	0.028			
N114	2	0.648 ± 0.044		1.870 ± 0.537		
R115	3	0.896 ± 0.025	91.198 ± 39.429			
C116	2	0.859 ± 0.045		0.651 ± 0.632		
Q117						
N118	2	0.897 ± 0.049		1.755 ± 0.755		
R119	3	0.737 ± 0.024	15.859 ± 2.560			
D120	4	0.658 ± 0.065	2,166.241 ± 811.066		0.820 ± 0.029	0.803 ± 0.029
V121	4	0.587 ± 0.059	1,677.012 ± 650.932		0.735 ± 0.030	0.799 ± 0.030
R122	4	0.777 ± 0.069	1,060.134 ± 543.849		0.943 ± 0.035	0.824 ± 0.035
Q123	3	0.808 ± 0.020	131.745 ± 32.861			
Y124	3	0.881 ± 0.025	21.842 ± 7.503			
V125	1	1.001 ± 0.027				
Q126	3	0.819 ± 0.025	25.927 ± 6.003			
G127	1	0.782 ± 0.025				
C128	1	0.788 ± 0.024				
G129	4	0.673 ± 0.065	1,673.584 ± 510.713		0.878 ± 0.031	0.766 ± 0.031
V130						

The internal motion of ligand-bound human lysozyme elucidated by ^{15}N spin relaxation

The relaxation parameters for $(NAG)_3$-bound human lysozyme were also measured (Fig. 4). We found that internal motions around active site regions significantly changed compared with those of the free state.

After an optimized value for τ_c of 5.63 ns was obtained, the model-free analysis was carried out using these relaxation parameters as described above. However, there were some signals that could not be analyzed due to extreme line broadening caused by the substantial conformational exchange for a large subset of residues. As a result, values of the internal motion parameters for 104 out of 130 main-chain amide groups were obtained (Fig. 5; Table 2B). Many residues were observed to change their internal motions upon binding of $(NAG)_3$. Significant increases in the order parameter, reflecting more restricted motion in the ligand-bound state, were located in strand 2 (D53), turn 2 (F57), long loop (A76), loop C–D (G105), and 3_{10} (ii) (V125). On the other hand, significant decreases in the order parameter, reflecting less restricted motion upon binding of the ligand, were located in turn 1 (A47, G48), long loop (N75, C77), 3_{10} (i) (A83), helix C (V93), helix D (N114), 3_{10} (ii) (R122), and the C-terminus (G129). The timescale of the interaction between human lysozyme and $(NAG)_3$ may be slower than that of the instrument employed here. Therefore, these exchange contributions are not caused by the exchange between free and $(NAG)_3$-bound enzyme because a substantial excess of substrate was added so that the fully complexed enzyme could form.

Discussion

Backbone dynamics of free human lysozyme: Compared with the internal motions of hen lysozyme

The analysis of the internal motion of hen lysozyme in solution has already been reported (Buck et al., 1995a). We also analyzed the backbone dynamics of hen lysozyme (Mine et al., 1999a), and our results were nearly consistent with the previous results. Here, we compared the internal motions between human and hen lysozyme, considering the insertion of a Gly residue at position 48 for human lysozyme relative to the sequence of hen lysozyme (Fig. 6A). The results indicated that the order parameters in the backbone, which reflect a ps-ns timescale of internal motion, were almost the same in each case. However, some residues were observed to significantly differ in mobility. Especially the mobility of the residues T70, Q86, and Q104 for human lysozyme, which correspond to T69, S85, and N103 for hen lysozyme, was much more restricted compared to the mobilities of those of hen lysozyme. It was suggested that some of the determinants of the dynamic behavior may correlate with neighboring residues in the protein sequence (Buck et al., 1995a); therefore, we compared the sequence around these three residues between human and hen lysozymes (Fig. 1). Judging from the comparison of sequence, a significant difference was found in sequence between Q104 and N103. In hen lysozyme, N103 lies between G102 and G104, while Q104 lies between P103 and G105 in human lysozyme. It is considered that the presence of a Gly residue contributes to high flexibility but a Pro residue is responsible for the reduction in mobility. Indeed, it was reported

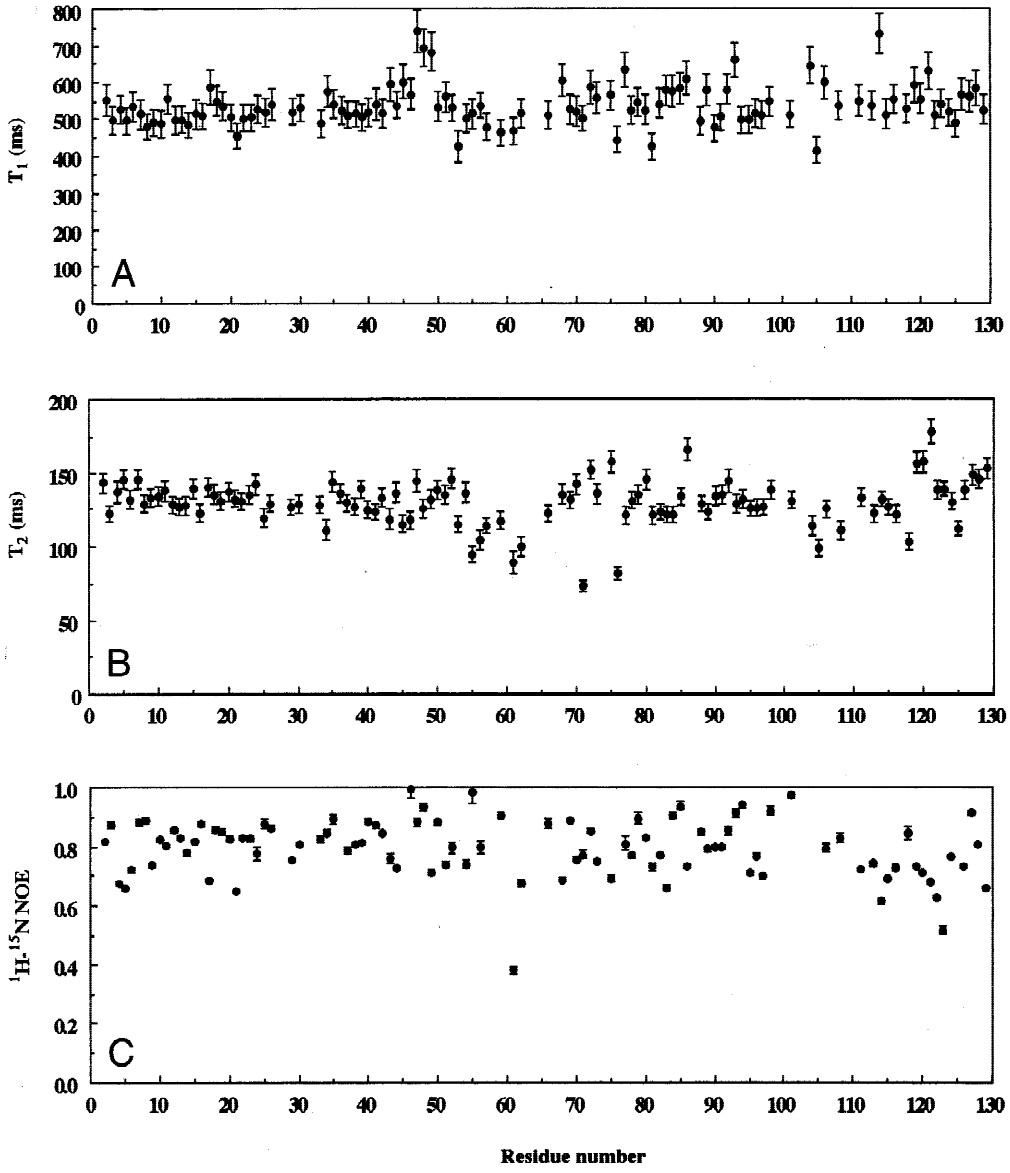

Fig. 4. (**A**) T_1, (**B**) T_2, and (**C**) heteronuclear NOE of the human lysozyme in the presence of $(NAG)_3$ at pH 3.8 and 35 °C.

that the substitution of Pro to Gly at position 103 resulted in the greater increase of the thermal factor at the mutated site compared to wild-type one (Herning et al., 1992). Therefore, this may be the reason why the backbone dynamics of Q104 in human lysozyme is more restricted than that of the corresponding residue in hen lysozyme. But we cannot understand the differences of mobilities of another two residues, T70 and Q86, by comparing the amino acid sequence.

It was reported that there was a case in which local hydrophobic packing interactions restricted the backbone dynamics (Eliezer et al., 1998). The total hydrophobicity was conserved in both lysozymes except for subtle differences in the packing of residues in the hydrophobic core (Hooke et al., 1994). Therefore, our results indicated that the efficiency of packing of the hydrophobic core had little effected on the internal motions. On the other hand, a molecular dynamics and model-free analysis of hen lysozyme suggested a significant relationship between fluctuations and surface accessibilities (Post et al., 1989; Buck et al., 1995a). When we also compared the relations between backbone dynamics and solvent accessibilities of human and hen lysozyme, those of both lysozymes are very similar as shown in Figure 7. In conclusion, the difference in the amino acid sequence between human and hen lysozyme was not the main determinant of dynamic properties, but the folded pattern of the protein was the most important property to dominate the internal motions of the protein.

Backbone dynamics of ligand-bound human lysozyme

It has been suggested that residues in the active site are mobile in the free state and that their motions become more highly restricted in a ligand-bound state to constrain the substrate to a conformation that resembles the transition state (Mildvan, 1974). In the present case, however, there were many residues whose order parameter decreased or increased in ligand-bound human lysozyme when we

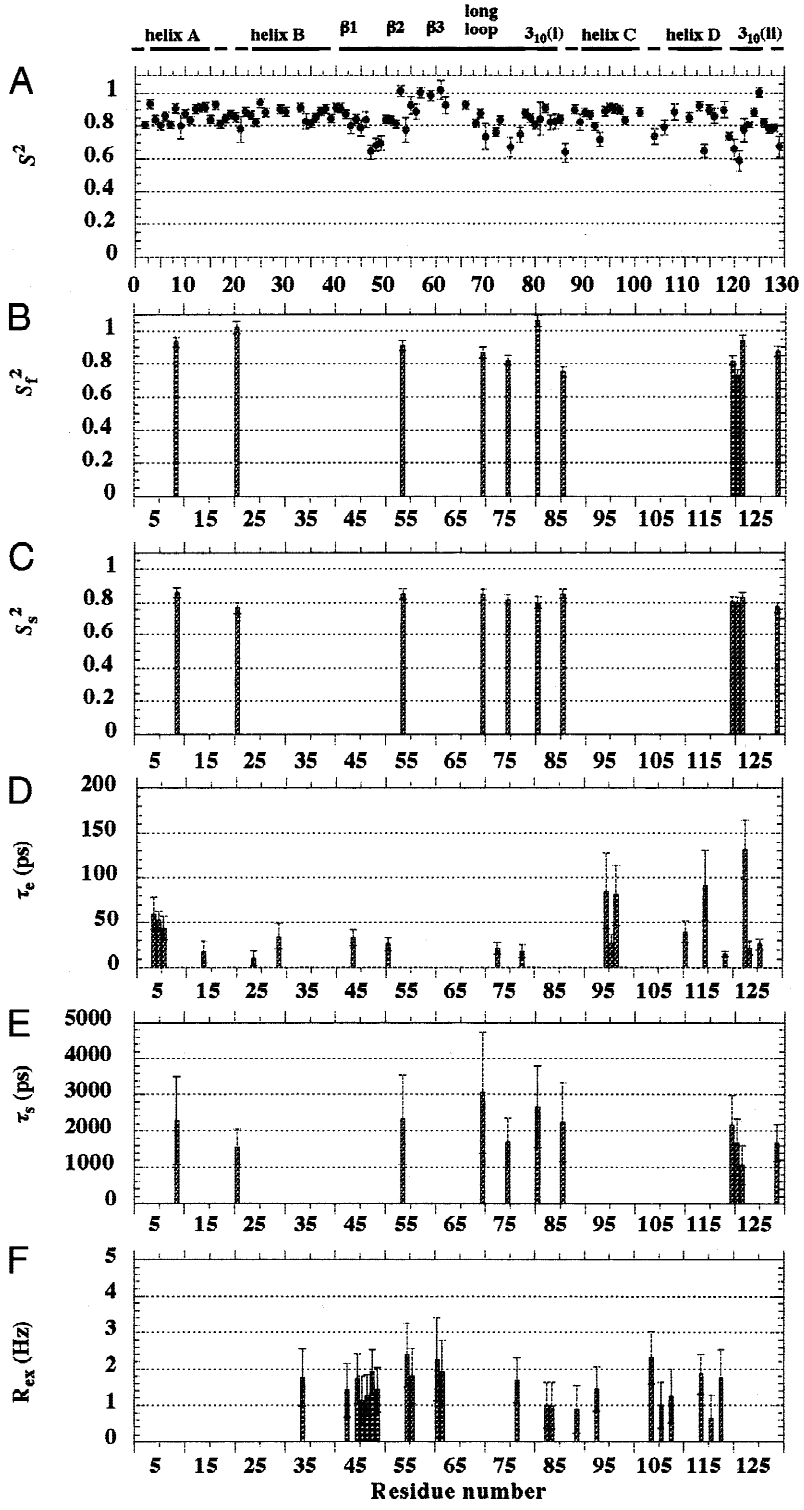

Fig. 5. Extracted model-free parameters of $(NAG)_3$-bound human lysozyme by parameter optimization with the program RxAnly. **A:** Generalized order parameters S^2. **B:** Order parameters of the fast internal motion S_f^2. **C:** Order parameters of the slow internal motion S_s^2. **D:** Effective correlation times τ_e. **E:** Slow internal correlation times τ_s. **F:** Chemical exchange contributions represented in the broadened linewidth R_{ex}.

compared these parameters with those in the unbound state (Fig. 8). This was consistent with the phenomena that were observed in the internal motions of ligand-bound hen lysozyme (Mine et al., 1999a) and mouse major urinary binding protein I (Zidek et al., 1999). Akke et al. (1993) demonstrated a simple relationship between contributions to the change in Gibbs free energy and order param-

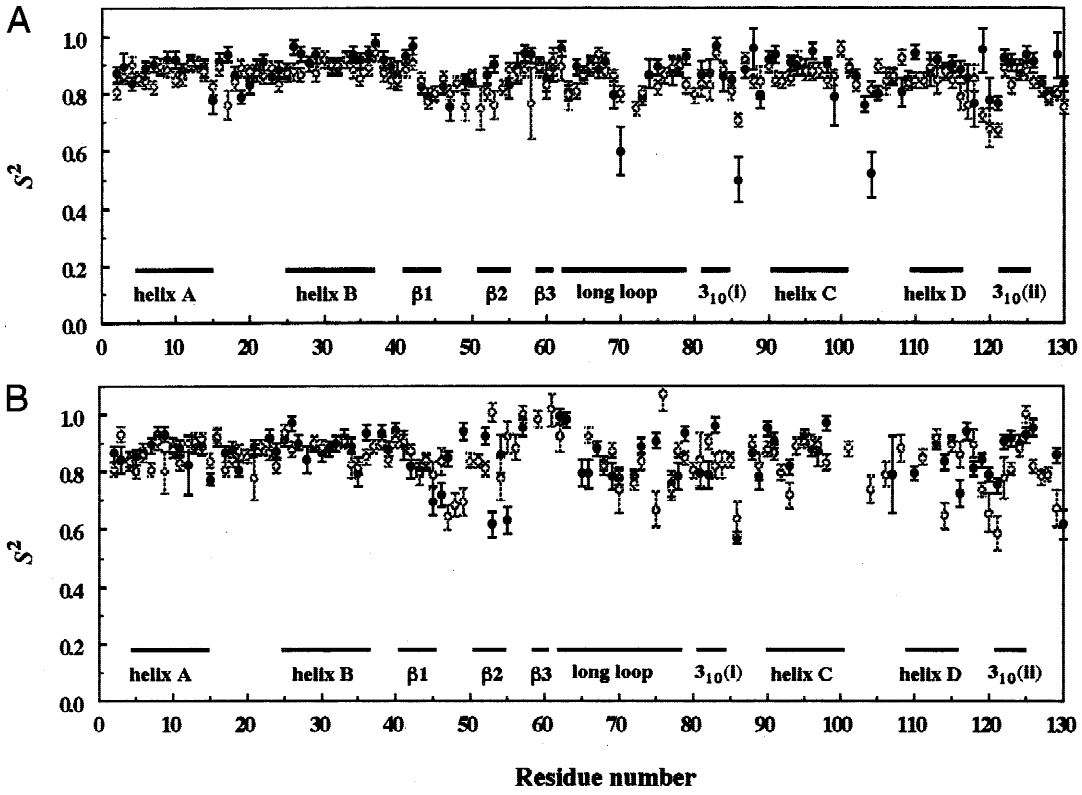

Fig. 6. Comparison of the generalized order parameters (S^2) for (**A**) free and (**B**) ligand-bound lysozyme. S^2 for hen lysozyme (closed circle) (Mine et al., 1999a) and human lysozyme (open circle).

eters derived from NMR measurement. Using this methodology, Stivers et al. (1996) found that, upon binding an inhibitor to 4-oxalocrotonate tautomerase, a number of residues showed a significant increase in order parameter while the others decreased, suggesting that the immobilization of a residue upon substrate or ligand binding resulted in an entropy penalty and the mobilization of other residues contributed to compensate for this penalty. These observations were consistent with our results obtained here. Moreover, it was notable that such residues were located not only at or near the active site regions but at the N-terminal region, which was far away from the active site (Fig. 8), indicating that the internal motion of the enzyme is closely involved in the substrate binding.

However, several differences in the dynamic behavior were clearly observed between ligand-bound human and hen lysozyme (Fig. 6B). As shown in Figure 9, these residues are mostly seen in helix B, C, strand 2, 3, and loop C–D, which are located at subsites A, B, C,

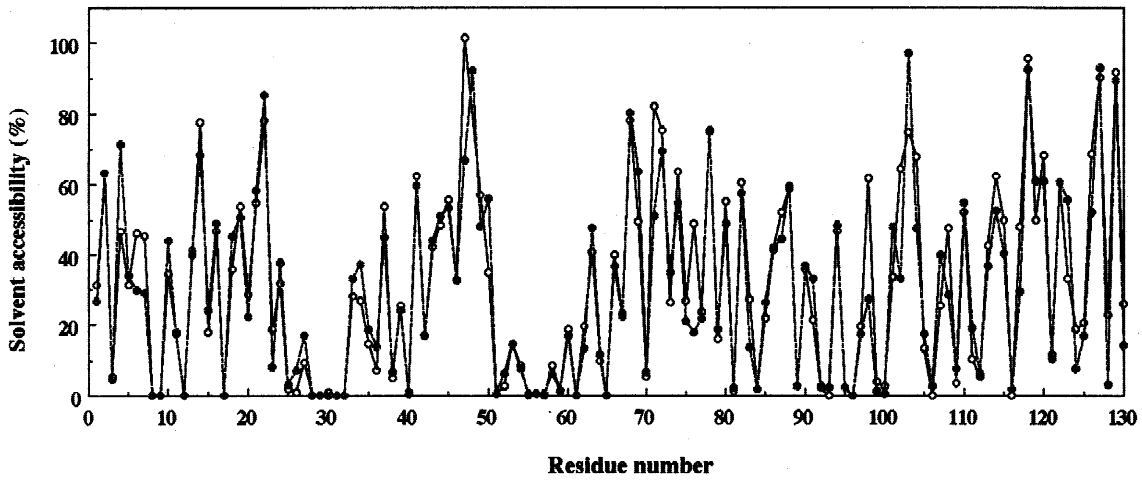

Fig. 7. Solvent accessibility of human (closed circle) and hen (open circle) lysozyme.

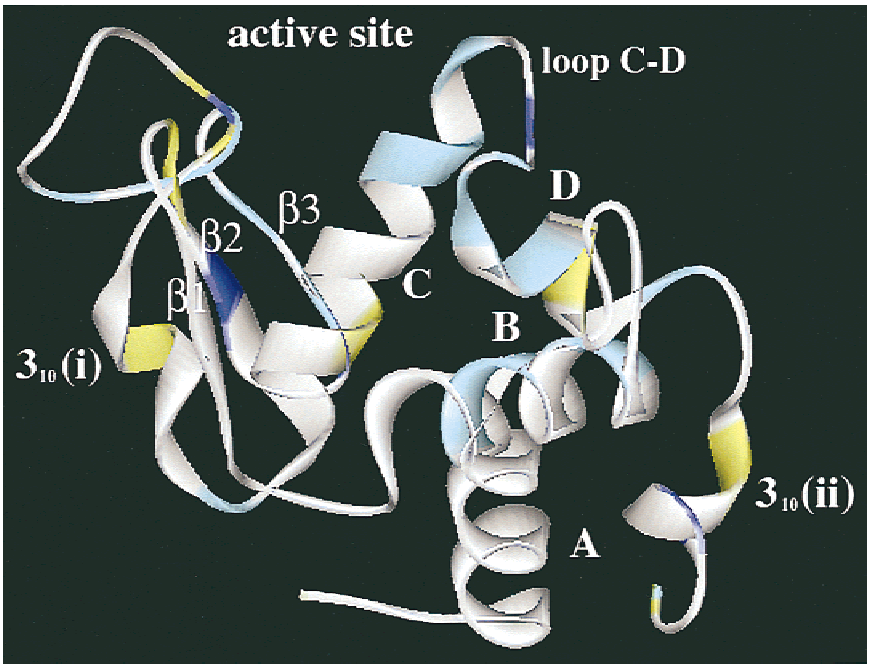

Fig. 8. Ribbon representation of human lysozyme showing regions with order parameter changed in the formation of complex with $(NAG)_3$. Residues with increase and decrease in order parameter are colored blue and yellow, respectively. The residues that could not be analyzed are colored light blue.

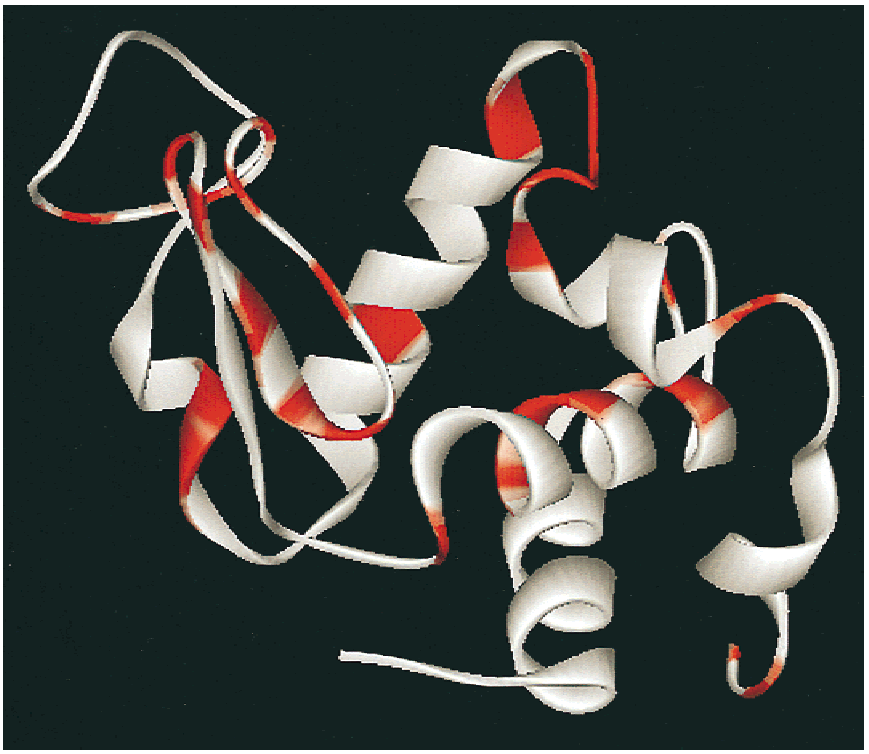

Fig. 9. Ribbon representation of human lysozyme showing regions with order parameter changed in the formation of complex with substrate analogue between human and hen lysozyme. Residues with increase and decrease in the values of order parameter over 0.2 are colored red.

and D. It was considered that these differences in dynamic behavior should arise from the differences in substrate binding mode or efficiency of activity toward glycol chitin between human and hen lysozyme. Human lysozyme was reported to bind $(NAG)_3$ in subsites A–C or in subsites B–D (Schindler et al., 1977; Matsushima et al., 1990), whereas hen lysozyme bound $(NAG)_3$ dominantly in subsites A–C (Blake et al., 1967; Imoto et al., 1972) (Fig. 10). This resulted from the residue at position 63 (corresponding to 62 for hen lysozyme), which is Y and W for human and hen lysozyme, respectively. In hen lysozyme, W62 is proposed to be involved in apolar interaction with a sugar ring bound to subsite B and hydrogen bonding to the hydroxyl oxygen atom of a sugar ring in subsite C (Blake et al., 1967; Cheetham et al., 1992), while in human lysozyme, Y63 might have reduced nonpolar interactions with the sugar ring in subsite B and lost hydrogen bonding to a sugar ring in subsite C, which might slightly change the binding mode of each subsite for sugar residues. Such situations might result in a difference in the binding mode between human and hen lysozyme, but a difference in this residue did not influence the enzymatic properties vs. the substrate analogue (Muraki et al., 1992).

It was reported that the structural details of the cleft lobe composed of the residues 100 to 105 was responsible for the turnover in the reaction of human lysozyme to the substrate (Muraki et al., 1997). Comparing S^2 values in Figure 5 of the present paper with those in Figure 9 of our previous paper (Mine et al., 1999a), it was clearly found that internal motions in several residues of the residues 100 to 115 in both $(NAG)_3$-bound lysozymes were different each other. In our previous paper (Mine et al., 1999a), we also showed the internal motions of the mutant hen lysozyme that has a higher activity toward the substrate. In the mutant hen lysozyme, the internal motions of several residues of the residues from 100 to 115 were also different compared to wild-type hen lysozyme. Therefore, it was suggested that the difference in internal motion in the lobe composed of residues 100 to 115 in lysozyme may be involved in the improvement of activity.

We should analyze the internal motion of human lysozyme in the presence of a longer substrate analogue such as $(NAG)_6$ when we discuss whether the internal motion was involved in biological function in vivo. However, since such a substrate is hydrolyzed during NMR measurement, we may not take advantage of it in this

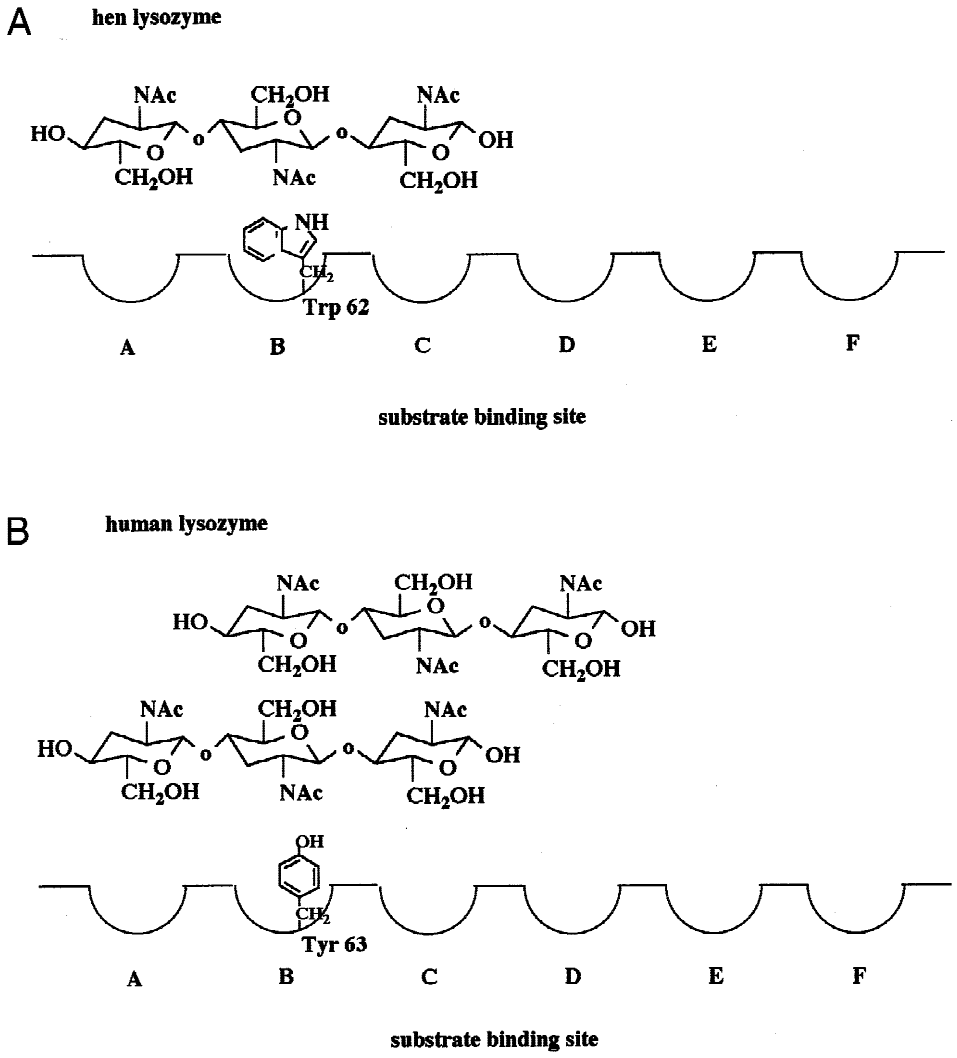

Fig. 10. The binding modes of $(NAG)_3$ in the active site cleft of (**A**) hen and (**B**) human lysozyme. A–F shows the subsites in the active site of both lysozymes.

experiment. Human lysozyme and the mutant hen lysozyme, which had a higher activity than hen lysozyme, were reported to have a larger association rate constant than hen lysozyme in the lysozyme-immobilized $(NAG)_3$ binding (Ueda et al., 1998), indicating that the binding of lysozyme to $(NAG)_3$ is related to the biological function of lysozyme.

Considering the above results, the larger association rate constant may be involved in the difference in internal motion in the lobe composed of residues 100 to 115 in human lysozyme. Thus, we suggested that this difference in mobility around the active site region between human and hen might be the reason for the difference in efficiency of activity.

In conclusion, the ^{15}N relaxation measurements have afforded detailed characterizations of backbone dynamics in the absence and presence of a substrate analogue. In the absence of $(NAG)_3$, the results presented here suggested that the entire dynamic properties of human and hen lysozyme were dominated by their folded patterns rather than by the amino acid sequence. In the presence of $(NAG)_3$, both lysozymes changed in the internal motions around the active site region to minimize the entropic disadvantage. These observations indicated a new aspect of enzyme-substrate binding mode, which is the so-called "induced fit." However, there were differences in the dynamic behavior of some regions between human and hen lysozyme upon $(NAG)_3$ binding. This may depend on the difference in binding mode in both lysozymes and the internal motion in the lobe composed of residues 100 to 115. In this study, by investigating the backbone dynamics between structurally homologous proteins, we could obtain extremely valuable indication of the key in the determinant of internal motions. Furthermore, subtle differences in substrate-binding subsite could be detected by relaxation analysis, and this may contribute to the recognition of the events in enzyme-substrate interactions. Anyway, the results indicate that the internal motion is closely related to the biological functions of proteins.

Materials and methods

Sample preparation

^{15}N-labeled human lysozyme was obtained from a *Pichia pastoris* expression system. The procedure of production and purification of ^{15}N-labeled lysozyme was the same as those described previously (Mine et al., 1999b). Finally, we obtained about 20 mg of ^{15}N-labeled lysozyme from 1 L of culture.

NMR measurements

The NMR sample was prepared to contain 1 mM protein in 90% H_2O/10% D_2O (v/v), and the pH was adjusted to 3.8. For preparation of the lysozyme complex, $(NAG)_3$ was added to the protein solution to yield a slight excess of substrate relative to the enzyme. Under this condition, more than 99% complex was formed. NMR experiments were performed at 35 °C on a Varian Inova 600 MHz spectrometer equipped with a triple-resonance, pulse-field gradient probe with an actively shielded z gradient and a gradient amplifier unit. The 3D ^{15}N-edited NOESY-HSQC (Marion et al., 1989) with a mixing time of 100 ms were collected with a time domain data size of 120 (t_1) × 30 (t_2) × 1,024 (t_3) complex points. Pulse sequences for the measurement of the ^1H–^{15}N NOE values, and the T_1 and T_2 relaxation times have been described previously (Kay et al., 1989; Kördel et al., 1992).

The ^{15}N T_1 values were determined from a series of ^1H–^{15}N correlation spectra with different relaxation durations, 32.94, 92.94, 172.94, 332.94, 652.94, 1,292.94, and 1,812.94 ms, while for the T_2 values, they were determined from the spectra with durations of 4, 42, 82, 122, 202, 282, and 342 ms. A recycle delay of 4.0 s was used for the T_1 relaxation and of 2.4 s for the T_2 experiments. The ^1H–^{15}N steady-state NOE values were determined from pairs of spectra, recorded with and without proton saturation. A recycle delay of 4.0 s was used for each NOE experiment. The spectra widths of the F_1 and F_2 dimensions were 3,647 Hz and 9,611 Hz, respectively. Each collected data set contained 256 (t_1) × 1,152 (t_2) complex data points.

Analysis of the relaxation parameters

All spectra were processed and analyzed using nmrPipe (Delaglio et al., 1995) and PIPP (Garrett et al., 1991). The peak intensities of each cross peak in a series of 2D data were extracted using nmrPipe based on the peak position defined by the contour averaging algorithm with the program PIPP. A series of extracted intensity profiles of each cross peak was used for the extraction of the T_1 and T_2 relaxation times, using a single exponential model function. The steady-state ^1H–^{15}N NOE values were determined from the ratios of the intensities of the peaks with and without proton saturation.

Model-free analysis

The relaxation data were analyzed using the model-free formalism of Lipari and Szabo (1982a, 1982b) and the extension of this method developed by Clore et al. (1990), as described Tate et al. (1998).

Acknowledgments

The authors thank Dr. Shin-ichi Tate (Japan Advanced Institute of Science and Technology, Hokuriku) for his valuable discussion, providing pulse sequence and data analysis programs.

References

Akke M, Skelton NJ, Kordel J, Palmer AG 3rd, Chazin WJ. 1993. Effects of ion binding on the backbone dynamics of calbindin D_9k determined by ^{15}N NMR relaxation. *Biochemistry 32*:9832–9844.

Artymuik PJ, Blake CCF. 1981. Refinement of human lysozyme at 1.5 Å resolution analysis of non-bonded and hydrogen-bond interactions. *J Mol Biol 152*:737–762.

Blake CC, Johnson LN, Mair GA, North AC, Phillips DC, Sarma VR. 1967. Crystallographic studies of the activity of hen egg-white lysozyme. *Proc R Soc Lond B Biol Sci 167*:378–388.

Boyd J, Redfield C. 1998. Defining the orientation of the ^{15}N shielding tensor using ^{15}N NMR relaxation data for protein in solution. *J Am Chem Soc 120*:9692–9693.

Buck M, Boyd J, Redfield C, MacKenzie DA, Jeenes DJ, Archer DB, Dobson CM. 1995a. Structural determinants of protein dynamics: Analysis of ^{15}N NMR relaxation measurements for main-chain and side-chain nuclei of hen egg white lysozyme. *Biochemistry 34*:4041–4055.

Buck M, Schwallbe H, Dobson CM. 1995b. Main-chain dynamics of a partially folded protein: ^{15}N NMR relaxation measurements of hen egg white lysozyme denatured in trifluoroethanol. *J Mol Biol 257*:669–683.

Cheetham JC, Artymuik PJ, Phillips DC. 1992. Refinement of an enzyme complex with inhibitor bound at partial occupancy. Hen egg-white lysozyme and tri-*N*-acetylchitotriose at 1.75 Å resolution. *J Mol Biol 224*:613–628.

Clore GM, Driscoll PC, Wingfield PT, Gronenborn AM. 1990. Analysis of the backbone dynamics of interleukin-1 beta using two-dimensional inverse detected heteronuclear ^{15}N-^1H NMR spectroscopy. *Biochemistry 29*:7387–7401.

Creighton CE. 1984. *Proteins*. New York: WH Freeman and Company. pp 105–138.

Delaglio F, Grzesiek S, Vuister GW, Zhu G, Pfeifer J, Bax A. 1995. NMRPipe: A multidimensional spectral processing system based on UNIX pipes. *J Biomol NMR 6*:277–293.

Eliezer D, Yao J, Dyson HJ, Wright PE. 1998. Structural dynamic characterization of partially folded states of apomyoglobin and implications for protein folding. *Nat Struct Biol 5*:148–155.

Gagne SM, Tsuda S, Spyracopoulos L, Kay LE, Sykes BD. 1998. Backbone and methyl dynamics of the regulatory domain of troponin C: Anisotropic rotational diffusion and contribution of conformational entropy to calcium affinity. *J Mol Biol 278*:667–686.

Garrett DS, Powers R, Gronenborn AM, Clore GM. 1991. A common sense approach to peak picking in two-, three-, and four-dimensional spectra using automatic computer analysis of contour diagrams. *J Magn Reson 95*:214–220.

Handoll H. 1985. D. Phil. Thesis. UK: Oxford University.

Herning T, Yutani K, Inaka K, Kuroki R, Matsushima M, Kikuchi M. 1992. Role of proline residues in human lysozyme stability: A scanning calorimetric study combined with X-ray structure analysis of proline mutants. *Biochemistry 31*:7077–7085.

Hooke SD, Radford SE, Dobson CM. 1994. The refolding of human lysozyme: A comparison with the structurally homologous hen lysozyme. *Biochemistry 33*:5867–5876.

Imoto T, Johnson LN, North ATC, Phillips DC, Rupley JA. 1972. *The enzyme*. 3rd ed. Vol. 7. New York: Academic Press. pp 665–868.

Kay LE, Torchia DA, Bax A. 1989. Backbone dynamics of proteins as studied by ^{15}N inverse detected heteronuclear NMR spectroscopy: Application to staphylococcal nuclease. *Biochemistry 28*:8972–8979.

Kördel J, Skelton NJ, Akke M, Palmer AG 3d, Chazin WJ. 1992. Backbone dynamics of calcium-loaded calbindin D_9k studied by two-dimensional proton-detected ^{15}N NMR spectroscopy. *Biochemistry 31*:4856–4866.

Kuramitsu S, Ikeda K, Hamaguchi K, Fujio H, Amano T. 1974. Ionization constants of Glu35 and Asp52 in hen, turkey, and human lysozymes. *J Biochem 76*:671–683.

Lipari G, Szabo A. 1982a. A model-free approach to the interpretation of nuclear magnetic resonance relaxation macromolecules I. Theory and range of validity. *J Am Chem Soc 104*:4546–4559.

Lipari G, Szabo A. 1982b. A model-free approach to the interpretation of nuclear magnetic resonance relaxation macromolecules II. Theory and range of validity. *J Am Chem Soc 104*:4559–4570.

Marion D, Driscoll PC, Kay LE, Wingfield PT, Bax A, Gronenborn AM, Clore GM. 1989. Overcoming the overlap problem in the assignment of ^{1}H NMR spectra of larger proteins by use of three-dimensional heteronuclear ^{1}H-^{15}N Hartmann-Hahn-multiple quantum coherence and nuclear Overhauser-multiple quantum coherence spectroscopy: Application to interleukin 1 beta. *Biochemistry 28*:6150–6156.

Matsushima M, Inaka K, Morikawa K. 1990. The structure of the human lysozyme-trisaccharide complex, refined with data by an "Imaging Plate" detector system. *Act Crystallogr A46*:C82.

Mildvan AS. 1974. Mechanism of enzyme action. *Annu Rev Biochem 43*:357–399.

Mine S, Tate S, Ueda T, Kainosho M, Imoto T. 1999a. Analysis of the relationship between enzyme activity and its internal motion using nuclear magnetic resonance: ^{15}N relaxation studies of wild-type and mutant lysozyme. *J Mol Biol 286*:1547–1565.

Mine S, Ueda T, Hashimoto Y, Tanaka Y, Imoto T. 1999b. High-level expression of uniformly ^{15}N-labeled hen lysozyme in *Pichia pastoris* and identification of the site in hen lysozyme where phosphate ion binds using NMR measurements. *FEBS Lett 448*:33–37.

Muraki M, Goda S, Nagahora H, Harata K. 1997. Importance of van der Waals contact between Glu 35 and Trp 109 to the catalytic action of human lysozyme. *Protein Sci 6*:473–476.

Muraki M, Harata K, Jigami Y. 1992. Dissection of the functional role of structural elements of tyrosine-63 in the catalytic action of human lysozyme. *Biochemistry 31*:9212–9219.

Ohkubo T, Taniyama Y, Kikuchi M. 1991. ^{1}H and ^{15}N NMR study of human lysozyme. *J Biochem 110*:1022–1029.

Post CB, Dobson CM, Karplus M. 1989. A molecular dynamics analysis of protein structural elements. *Proteins 5*:337–354.

Prompers JJ, Groenewegen A, Hilbers CW, Pepermans HA. 1999. Backbone dynamics of Fusarium solani pisi cutinase probed by nuclear magnetic resonance: The lack of interfacial activation revisited. *Biochemistry 38*:5315–5327.

Schindler M, Assaf Y, Sharon N, Chipman DM. 1977. Mechanism of lysozyme catalysis: Role of ground-state strain in subsite D in hen egg-white and human lysozymes. *Biochemistry 16*:423–431.

Schwalbe H, Fiebig KM, Buck M, Jones JA, Grimshaw SB, Spencer A, Glaser SJ, Smith LJ, Dobson CM. 1997. Structural and dynamical properties of a denatured protein. Heteronuclear 3D NMR experiments and theoretical simulations of lysozyme in 8 M urea. *Biochemistry 36*:8977–8991.

Stivers JT, Abeygunawardana C, Mildvan AS. 1996. ^{15}N NMR relaxation studies of entropy changes of an enzyme upon inhibitor binding. *Biochemistry 35*:16036–16047.

Tate S, Ohno A, Seeram SS, Hiraga K, Oda K, Kainosho M. 1998. Elucidation of the mode of interaction of thermolysin with a proteinaceous metalloproteinase inhibitor, SMPI, based on a model complex structure and a structural dynamics analysis. *J Mol Biol 282*:435–446.

Tjandra N, Feller SE, Pastor RW, Bax A. 1995. Rotational diffusion anisotropy of human ubiquitin from ^{15}N NMR relaxation. *J Am Chem Soc 117*:12562–12566.

Tjandra N, Wingfield P, Stahl S, Bax A. 1996. Anisotropic rotational diffusion of perdeuterated HIV protease from ^{15}N NMR relaxation measurements at two magnetic fields. *J Biomol NMR 8*:273–284.

Ueda T, Tsurumaru M, Imoto T. 1998. Kinetic measurement of the interaction between a lysozyme and its immobilized substrate analogue by means of surface plasmon resonance. *J Biochem 124*:712–716.

Wong KB, Daggett V. 1998. Barstar has a highly dynamic hydrophobic core: Evidence from molecular dynamics simulations and nuclear magnetic resonance relaxation data. *Biochemistry 37*:11182–11192.

Zhang W, Smithgall TE, Gmeiner WH. 1998. Self-association and backbone dynamics of the hck SH2 domain in the free and phosphopeptide-complexed forms. *Biochemistry 37*:7119–7126.

Zidek L, Novotny MV, Stone MJ. 1999. Increased protein backbone conformational entropy upon hydrophobic ligand binding. *Nat Struct Biol 6*:1118–1121.